INTERNATIONAL JOURNAL FOR NUMERICAL METHODS IN FLUIDS, VOL. 25, 1301–1313 (1997)

A STUDY OF AUTONOMOUS UNDERWATER VEHICLE HULL FORMS USING COMPUTATIONAL FLUID DYNAMICS

T. SARKAR, P. G. SAYER* AND S. M. FRASER

University of Strathclyde, 100 Montrose Street, Glasgow G4 0LZ, U.K.

SUMMARY

Reduction of the propulsive power requirement by efficient hull form design is one of the important requirements for the successful operation of autonomous underwater vehicles (AUVs). In the absence of reliable and sufficiently accurate experimental data this will require experimental analysis of a large number of hull forms, a task which is both expensive and time-consuming. Recent developments in computational fluid dynamics (CFD) can offer a cost-effective solution to this problem. In this paper such a method is developed to simulate the flow past axisymmetric AUVs. Its application is discussed for four different hull forms. © 1997 John Wiley & Sons, Ltd.

Int. J. Numer. Meth. Fluids, **25**: 1301–1313 (1997)

No. of Figures: 8. No. of Tables: 7. No. of References: 15.

KEY WORDS: autonomous underwater vehicles; CFD; drag; laminar and turbulent flows; numerical modelling

INTRODUCTION

In the last two decades, different areas of incompressible flow modelling, including grid generation techniques, solution algorithms, turbulence modelling and computer hardware capabilities, have witnessed tremendous developments. All these have led to the stage where it is now possible to consider the application of flow simulation techniques for use in complex aero- and hydrodynamic flow analysis. This is particularly true in those cases where an experimental database is scarce or incomplete. In this respect, hydrodynamic analysis of autonomous underwater vehicles (AUVs) under development forms an important application area of flow simulation techniques. The lack of a well-developed experimental database means that a large number of alternatives have to be studied in search of a low-drag AUV hull form. Much insight and guidance can be obtained efficiently and cost-effectively by flow simulation techniques.

A review by Patel and Chen[1] of post-1986 methods shows that some advances have been made in the development of calculation procedures for the complex flow past axisymmetric bodies which are typical of long-range AUV hull forms. Among the latter methods are those of Patel and Chen,[1] Park *et al.*[2] and Choi and Chen.[3] Most of these methods (except that of Choi and Chen), however, either use a simplified form of the governing equations e.g. boundary layer, thin layer or partially parabolic techniques, or try to simulate the flow near the tail region ($X/L \geqslant 0{\cdot}6$). Furthermore, they have not

* Correspondence to: P. G. Sayer, University of Strathclyde, 100 Montrose Street, Glasgow G4 0LZ, U.K.

Contract grant sponsor: Government of India, Ministry of Human Resource Development.

CCC 0271–2091/97/111301–13 $17.50

Received April 1996
Revised March 1997

been tested adequately for design applications. Even Choi and Chen's method, which uses a fully elliptic form of the governing equations and a k–ε model of turbulence, failed to produce numerically stable results for bodies such as MS, X-35 and F-57 (Figure 1) which have moderate curvature. This precludes its use in design.

Hence there is a need to develop a method using the elliptic form of the governing equations with a least a k–ε model of turbulence for simulating the complex flow past axisymmetric AUVs. For use in design the method needs to be computationally efficient, numerically stable and rigorously tested against available experimental results.

In this paper the development is reported of such a method based on the general-purpose proprietary software PHOENICS. After stating details governing equations, grid generation, boundary conditions and solution procedures, the selection of test cases is explained. This is followed by a discussion and analysis of the results to demonstrate the suitability of the present technique for use in design. Finally, conclusions are drawn and recommendations are made for future studies. Analysis of the results shows that the method is numerically robust, accurate enough for hull form design and computationally at least four times more efficient than the only other method (of Choi and Chen) used so far for simulation of the flow past the *entire length* of an axisymmetric body.

GOVERNING EQUATIONS

The governing equations for the flow past an axisymmetric AUV hull form are given below. Initially a standard k–ε model of turbulence with wall laws was used. For further improvement of the capability of the simulation technique this was then replaced by a low-*Re* Lam and Bremhorst (L&B)[4] k–ε model. This allowed integration down to the wall and so provided the simulation technique with an ability to detect transition, dispensing with wall laws which are not valid near the aft end of axisymmetric bodies, where the viscous sublayer becomes thicker than when subject to uniform stress conditions.

In cylindrical co-ordinates the governing equations can be expressed as

$$\frac{\partial}{\partial x}(\rho r u) + \frac{\partial}{\partial r}(\rho r v) = 0, \tag{1}$$

$$\frac{\partial}{\partial t}(\rho r \phi) + \frac{\partial}{\partial x}(\rho r u \phi) + \frac{\partial}{\partial r}(\rho r v \phi) = \frac{\partial}{\partial x}\left(r\Gamma_\phi \frac{\partial \phi}{\partial x}\right) + \frac{\partial}{\partial r}\left(r\Gamma_\phi \frac{\partial \phi}{\partial r}\right) + rS_\phi, \tag{2}$$

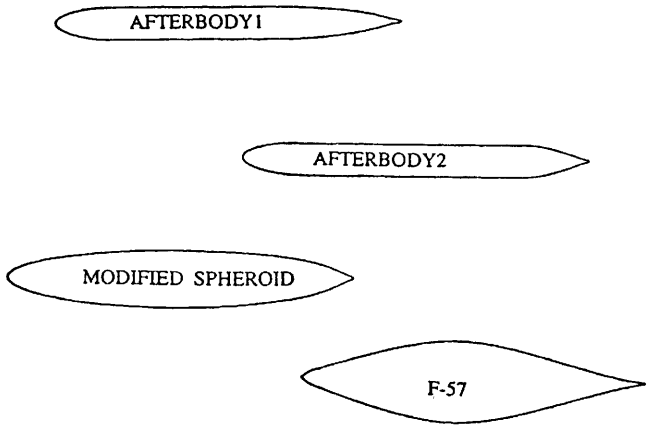

Figure 1. Selected test hull forms

Table I. Definition of variables

ϕ	Γ_ϕ	S_ϕ
u	$\mu+\mu_t$	$-\dfrac{\partial p}{\partial x}+\dfrac{\partial}{\partial x}\left(\mu_{\text{eff}}\dfrac{\partial u}{\partial x}\right)+\dfrac{1}{r}\dfrac{\partial}{\partial r}\left(r\mu_{\text{eff}}\dfrac{\partial v}{\partial r}\right)-\dfrac{2}{3}\dfrac{\partial k}{\partial x}$
v	$\mu+\mu_t$	$-\dfrac{\partial p}{\partial r}+\dfrac{\partial}{\partial x}\left(\mu_{\text{eff}}\dfrac{\partial u}{\partial r}\right)+\dfrac{1}{r}\dfrac{\partial}{\partial r}\left(r\mu_{\text{eff}}\dfrac{\partial v}{\partial r}\right)-2\mu_{\text{eff}}\dfrac{v}{r^2}$
k	$\mu+\dfrac{\mu_t}{\sigma_k}$	$G-\rho\varepsilon$
ε	$\mu+\dfrac{\mu_t}{\sigma_\varepsilon}$	$C_{\varepsilon1}f_1G\dfrac{\varepsilon}{k}-\rho C_{\varepsilon2}f_2\dfrac{\varepsilon^2}{k}$

where ϕ represents general dependent variables (u, v, k, ε), (u, v) are the velocity components in directions (x, r), ρ is the density of the fluid, Γ_ϕ is the effective diffusion coefficient and S_ϕ denotes the source for the variable. The definitions of the variables are given in Table I, where

$$\mu_{\text{eff}}=\mu+\mu_t, \qquad \mu_t=C_\mu f_\mu\rho\frac{k^2}{\varepsilon},$$

$$G=\mu_{\text{eff}}\left[2\left(\frac{\partial u}{\partial x}\right)^2+2\left(\frac{\partial v}{\partial r}\right)^2+2\left(\frac{v}{r}\right)^2+\left(\frac{\partial u}{\partial r}+\frac{\partial v}{\partial x}\right)^2\right],$$

$$C_{\varepsilon1}=1{\cdot}44, \quad C_{\varepsilon2}=1{\cdot}92, \quad C_\mu=0{\cdot}09, \quad \sigma_k=1{\cdot}0, \quad \sigma_\varepsilon=1{\cdot}3,$$

$$R_{\text{T}}=\frac{k^2}{v\varepsilon}, \qquad R_y=\frac{k^{1/2}y}{v}, \qquad f_\mu=[1-\exp(-0{\cdot}0165R_y)]^2,$$

$$f_1=1+\left(\frac{0{\cdot}05}{f_\mu}\right)^3, \qquad f_2=1-\exp(-R_{\text{T}}^2),$$

with y as the normal distance from the body wall.

In the standard k–ε model the low-Re constants f_1, f_2 and f_μ are set equal to one.

GRID GENERATION

A body-fitted H-type grid was obtained by numerical solution of the Poisson equations. The grid independence of the results was assessed by the h^m method outlined in Reference 5. In total, 171 grids were used in the x-direction. The numbers of grids in the x-direction (NG) and the grid expansion ratios (GE) used for different regions are shown in Figure 2.

In the r-direction the grids were made finer near the wall, in the laminar sublayer, to resolve adequately this thin layer of high velocity gradient. Approximately 15 control volumes were located within the viscous region $y^+ < 10$. The first grid node was located at y^+ between 0·5 and 0·8, depending on the type of body and the axial location. In total, 49 grids for AFTERBODY1 and 48 grids for AFTERBODY2 were used in the r-direction, of which the first 10 were at a uniform spacing $\Delta y^+ = 0{\cdot}5$. The next 10 co-ordinates were obtained by using an expansion ratio of 1·2 and thereafter an expansion ratio of 1·3 was used. A typical grid lay-out near AFTERBODY1 is shown in Figure 3. A summary of the grids for the four bodies under test is given in Table II.

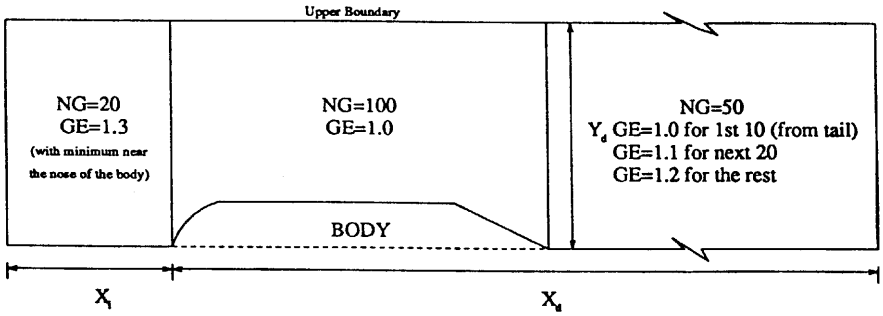

Figure 2. Grid details

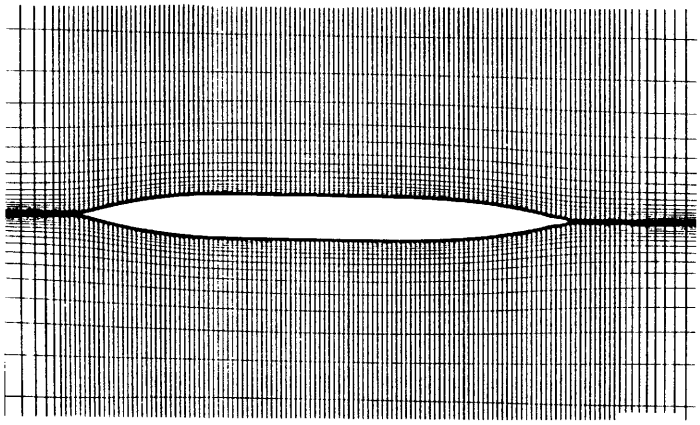

Figure 3. Grid lay-out near AFTERBODY1

Table II. Grid details

Type of body	Grid		X_i (starting point)	X_d (end point)	Y_u (top point)
	High-*Re*	Low-*Re*			
AFTERBODY1	171×36	171×48	$-2{\cdot}23$	$16{\cdot}80$	$1{\cdot}77$
AFTERBODY2	171×36	171×48	$-2{\cdot}23$	$16{\cdot}80$	$1{\cdot}80$
MS	171×36	171×49	$-2{\cdot}23$	$16{\cdot}80$	$1{\cdot}02$
F-57	171×36	171×49	$-2{\cdot}23$	$16{\cdot}80$	$1{\cdot}18$

BOUNDARY CONDITIONS

For solution of the governing equations it is necessary to specify boundary and initial conditions. In the present method, boundary conditions are incorporated in the finite volume equations by additional source and sink terms. Two sets of boundary conditions were used according to whether the near-wall viscous region was bridged using a wall law or the low-*Re* L&B model. For simulations using a wall law, the boundary conditions are as follows.

(a) At the inlet:

$$u = u_{\mathrm{i}}, \qquad k = k_{\mathrm{i}}, \qquad \varepsilon = \varepsilon_{\mathrm{i}},$$

with

$$k_{\mathrm{i}} = 1{\cdot}5(Tu)^2, \qquad \varepsilon_{\mathrm{i}} = C_{\mu}\frac{k_{\mathrm{i}}^{1{\cdot}5}}{l_{\mathrm{i}}},$$

turbulent intensity $Tu = 0{\cdot}5\%$ and length scale $l_{\mathrm{i}} = 0{\cdot}001L$ (L is the length of the body), as per Choi and Chen.

(b) At the downstream boundary: $p = 0$.

(c) On the body surface: u, v, k and ε are specified by the wall functions of Launder and Spalding.[6]

(d) On the upper boundary: $u = u_{\mathrm{i}}$.

(e) At the centreline (except on the body itself): $v = 0$ and $u_{\mathrm{r}} = k_{\mathrm{r}} = \varepsilon_{\mathrm{r}} = 0$.

For the simulations using the low-*Re* L&B model, the above boundary conditions hold except on the body wall, where the log-law wall functions are replaced by the following conditions at the wall:

$$u = 0, \qquad k = 0, \qquad \frac{\partial \varepsilon}{\partial y} = 0.$$

SOLUTION PROCEDURE

All the conservation equations for mass, momentum, k and ε can be expressed in the form of a general transport equation for an arbitrary dependent variable ϕ as

$$\frac{\partial}{\partial t}(\rho\phi) + \frac{\partial}{\partial x_i}(\rho U_i \phi) = \frac{\partial}{\partial x_i}\left(\Gamma_{\phi}\frac{\partial \phi}{\partial x_i}\right) + S_{\phi}. \tag{3}$$

This general form of the governing equations is translated into a set of linear algebraic equations. In the present method this is achieved using a finite volume technique by dividing the computational domain into a number of control volumes or cells. The control volumes used for the current work are arbitrary curvilinear, with the body surfaces coinciding with the boundaries of the flow domain. The finite volume equations of a variable at a cell are derived by writing down the convective and diffusive fluxes across each face of the cell, summing them over all the faces and adding any source term which may be present within the cell. These involve interpolation assumptions which in the present method correspond to 'fully implicit' and 'hybrid' formulations. Details of these formulations are available in Reference 7.

In algebraic form the relationship for the steady axisymmetric case can be written as

$$a_{\mathrm{P}}\phi_{\mathrm{P}} = a_{\mathrm{N}}\phi_{\mathrm{N}} + a_{\mathrm{S}}\phi_{\mathrm{S}} + a_{\mathrm{L}}\phi_{\mathrm{L}} + a_{\mathrm{H}}\phi_{\mathrm{H}} + b, \tag{4}$$

where the subscript P denotes 'grid point', subscripts N, S, H and L denote 'neighbours' and b represents the relevant source term. The coefficients a express the influence of convection and diffusion across all boundaries. This equation is the finite volume equivalent of the governing differential equation for the flow past axisymmetric bodies, which is solved by using the 'staggered grid' method[7] and 'SIMPLEST' algorithm.[8] The equations were solved by repeated sweeps in the flow direction. Very good convergence (residue $< 1{\cdot}0 \times 10^{-5}$) was obtained after 500 iterations. However, approximately 1000–1200 sweeps were performed to allow free development of the wake. Also for each sweep, about 20 iterations of the linear equation solver for pressure at each slab were required to achieve convergence. To promote numerical stability, linear relaxation was used for the

pressure and the method of 'false time step' was used for the velocity and turbulence parameters. Details of these are available in Reference 9.

COMPUTING RESOURCES

The computing resources are now considered. A comparison of the computing time required for the present method is given in Table III against that of Chen and Choi's method. Flow was simulated on a Sparc 10/514 machine with four processors working at 55 MHz. However, the programme used only one processor solely dedicated to the job.

Table III shows that the present method, which uses a much simplified formulation of a one-velocity staggered grid approach rather than the more elaborate two-velocity staggered grid approach of Chen and Choi, is at least four times faster than the latter. Hence there are potential benefits in using the developed technique for numerical simulation of the flow past AUVs.

Test runs of the method on a PC with an Intel Pentium processor operating at 90 MHz required only 3500 s to complete a single run. Considering that such a PC is now widely available, this method does not need any sophisticated computing facility and is highly portable (extending the technique to 3D modelling will, however, require extensive computing resources).

SELECTION OF TEST CASES

To test the method, simulations were undertaken for the flow past four different axisymmetric hull forms: AFTERBODY1, AFTERBODY2, MS and F-57 (Figure 1).

The reasons for the choice of these hull forms were two fold. First, they are representative of a wide spectrum of shapes ranging from typical torpedo forms with a cylindrical middle body to low-drag bodies having strong surface curvature. Secondly, for these bodies, reliable experimental data are already available for rigorous testing of numerical simulation results (e.g. References 10–12) at the following Re: AFTERBODY1, $Re = 6{\cdot}6 \times 10^6$, AFTERBODY2, $Re = 6{\cdot}8 \times 10^6$, F-57, $Re = 6{\cdot}6 \times 10^6$, MS, $Re = 6{\cdot}6 \times 10^6$.

RESULTS AND DISCUSSION

Surface pressure coefficients, friction velocity and overall volumetric drag coefficients are important quantities for assessing the hydrodynamic efficiency of AUV hull forms. Hence any method developed for numerical simulation of the flow past AUVs should have the capability to predict these quantities with reasonable accuracy. The above test cases are now analysed.

Figures 4(a)–4(d) present surface pressure plots using the L&B model and the standard k–ε model plus wall functions. The results are compared with the experimental results of Huang *et al.*,[10] Patel and Lee[11] and Patel *et al.*[12] For AFTERBODY1 and AFTERBODY2, comparison was also made against the numerical results of Choi and Chen,[3] who used a high-Re k–ε model for turbulence. The

Table III. Comparison of computing times

	Time (s)		
Type of method	Grid generation	Solution	Total
Present technique	28·2	2403·0	2431·2
Chen and Choi's method	28·2	11350·1	11378·3

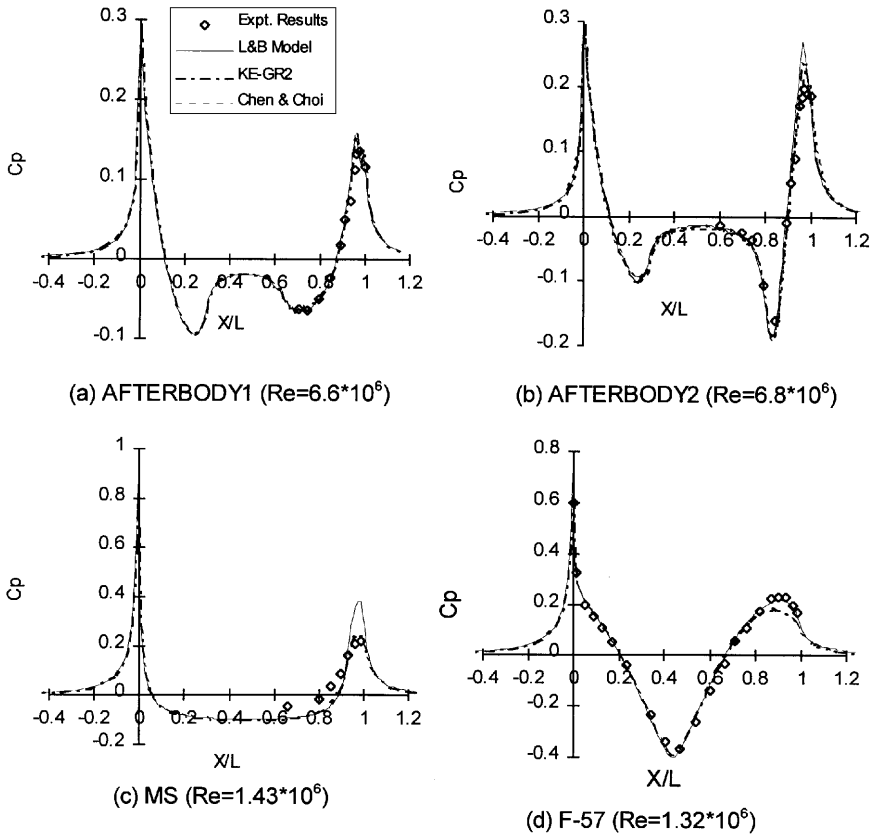

Figure 4. Surface pressure coefficient plots

comparisons are very good, except for the last 5–10% of the length. In this region, for MS and AFTERBODY2, the L&B model generated higher values of the pressure coefficient; the standard model with wall functions seems to show better agreement with the experimental data. This is due to the large radial pressure gradients near the hull surface and the inability of the pitot static tubes used in the experiments to measure the pressure exactly at the hull surface. For F-57, accurate pressure measurements were obtained using surface taps; the best numerical comparison was obtained with the L&B model. These figures also show that the results of the present method using a high-*Re* version of the k–ε model are of comparable accuracy to Chen and Choi's method, which uses the computationally intensive two-velocity staggered grid approach of Maliska and Raithby.[13]

Figures 5(a)–5(d) show the corresponding friction velocity plots. The apparently better agreement with the standard model with wall functions for F-57 and MS can be explained by the fact that the experimental data were obtained using Clauser plots, which assume validity of the same wall law. However, wall functions are not valid for F-57 and MS because of their large hull curvatures. Hence those experimental results are questionable. The better agreement between the experimental data and results from the low-*Re* k–ε model for AFTERBODY1 and AFTERBODY2 can be explained in the same way: owing to the longer length of the parallel middle body, the flow past these bodies is closer to the equilibrium turbulent flow where wall functions are valid. For the low-*Re* k–ε model, localized increases in the friction velocity, observed near the stagnation point of all four bodies, are due to excessively large returns of turbulent scale in this region by the L&B model. This adversely affects

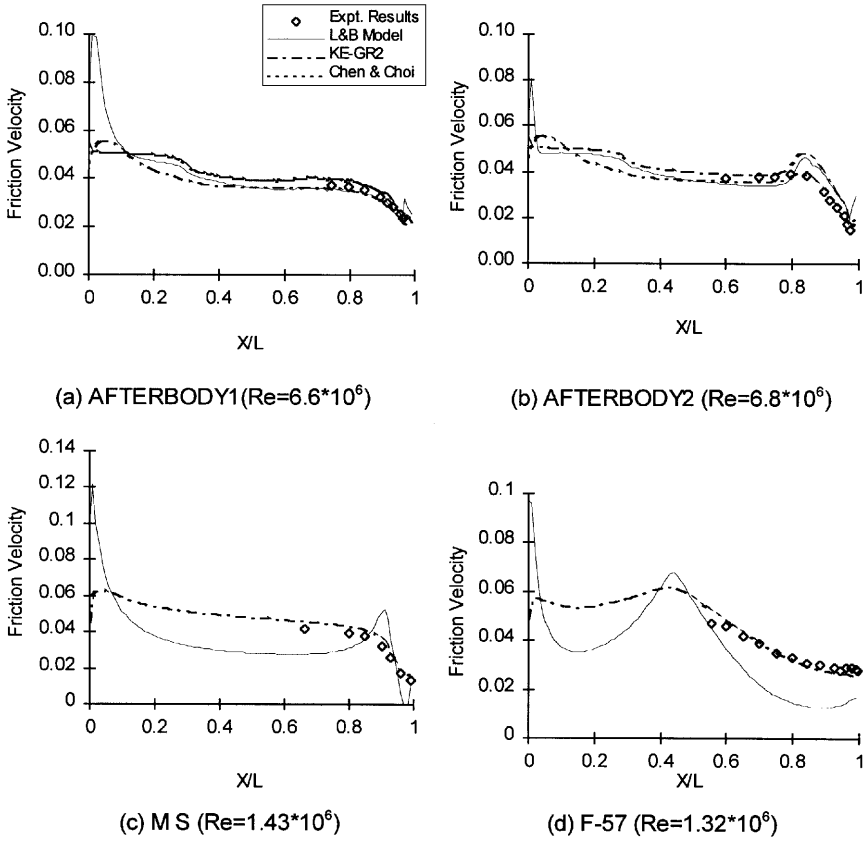

Figure 5. Friction velocity plots

the prediction of the drag. To remove this inadequacy, the corrections proposed by Yap[14] were applied to the present technique. These corrections require the addition of an extra source term in the ε-equation. The volumetric source term takes the form

$$S_\varepsilon = \max(0{\cdot}83\rho(l/l_e - 1{\cdot}0)(l/l_e)^2\varepsilon^2/k, 0), \tag{5}$$

with $l = k^{1{\cdot}5}/\varepsilon$ and $l_e = [(C_\mu)^{0{\cdot}75}\kappa]y$, where y is the distance from the wall, $C_\mu = 0{\cdot}09$ and $\kappa = 0{\cdot}435$.

This term vanishes in the local equilibrium condition, because then $l = l_e$; it also becomes small or zero at large distances from the wall or in laminar regions, since $l < l_e$. However, if $l > l_e$, (5) is positive, leading to increased values of ε and reduced values of turbulent length scale l.

Figures 6(a)–6(d) show the friction velocities after application of the Yap corrections. The large returns of turbulent length scale are reduced for AFTERBODY1 and AFTERBODY2. However, there is no improvement for MS and F-57, because the flow in these cases is laminar and hence not affected by the Yap corrections.

Pressure and velocity profiles are given in Figures 7 and 8 respectively for AFTERBODY1 using the L&B model and the standard model with wall functions. The results compare well with the experimental values. These figures also show that the pressure results are almost identical for both the L&B and standard k–ε models, whereas in the case of velocity there is a definite improvement when

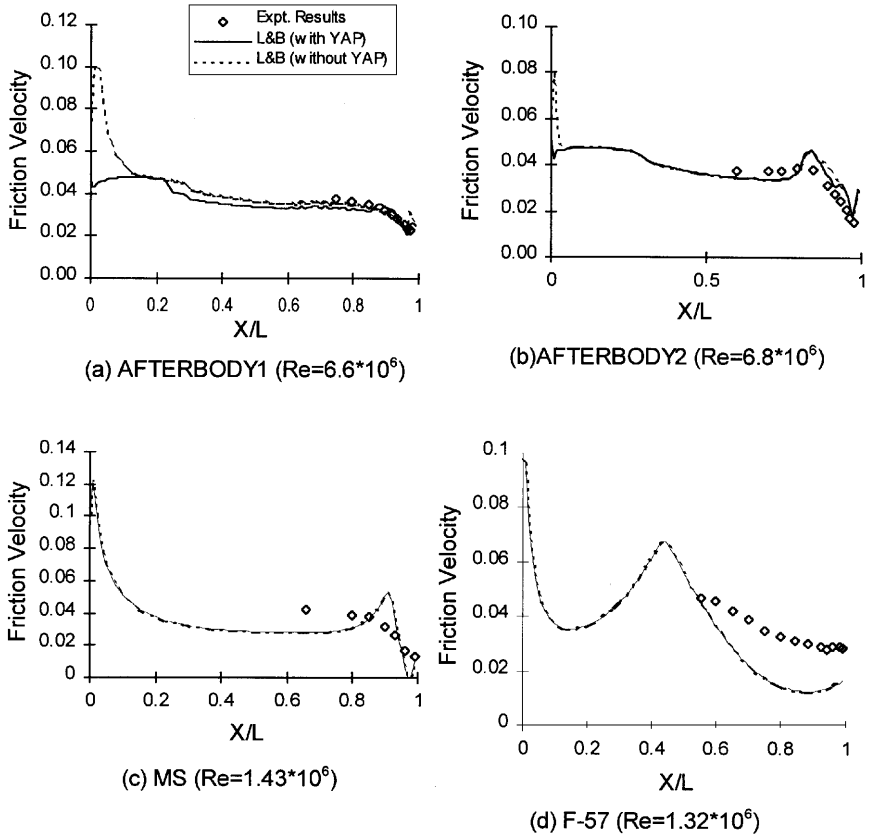

Figure 6. Friction velocity with Yap corrections

using the L&B model. Here also the results from the present method using a high-*Re* k–ε model are of comparable accuracy to those obtained by Chen and Choi's method.

Volumetric drag coefficients are compared with those obtained from ESDU[15] and, where available, experimental results, for example, see Tables IV–VII. The ESDU formulae work quite well for torpedo-shaped bodies. For the other two bodies, in the absence of available experimental data, the ESDU formulae were used only as a guide.

This comparison also shows that the L&B model improves the agreement with the ESDU results and experimental data for AFTERBODY1 and AFTERBODY2. For MS the pressure and friction components predicted by the L&B model are almost half those predicted by the standard model. The differences come from the ability of the L&B model to resolve the flow details very close to the surface of the body. This capability helps to capture more accurately the higher value of surface pressure near the aft end and the lower value of friction for $0{\cdot}1 < X/L < 0{\cdot}8$. (Values predicted by ESDU are not of much importance here; as already mentioned, the method was not proposed for this type of body.) Similar trends are also observed for F-57. Application of the L&B model alone, however, resulted in an anomaly in drag prediction of AFTERBODY1, leading to a large value of C_{dv} than for AFTERBODY2. This is in contrast with the experimental results and predictions by the standard k–ε model. This discrepancy is due to the results being affected by the large return of turbulent length scale over a larger proportion of AFTERBODY1 than AFTERBODY2. As evident in Tables IV–VII, this anomaly was removed by application of the Yap corrections.

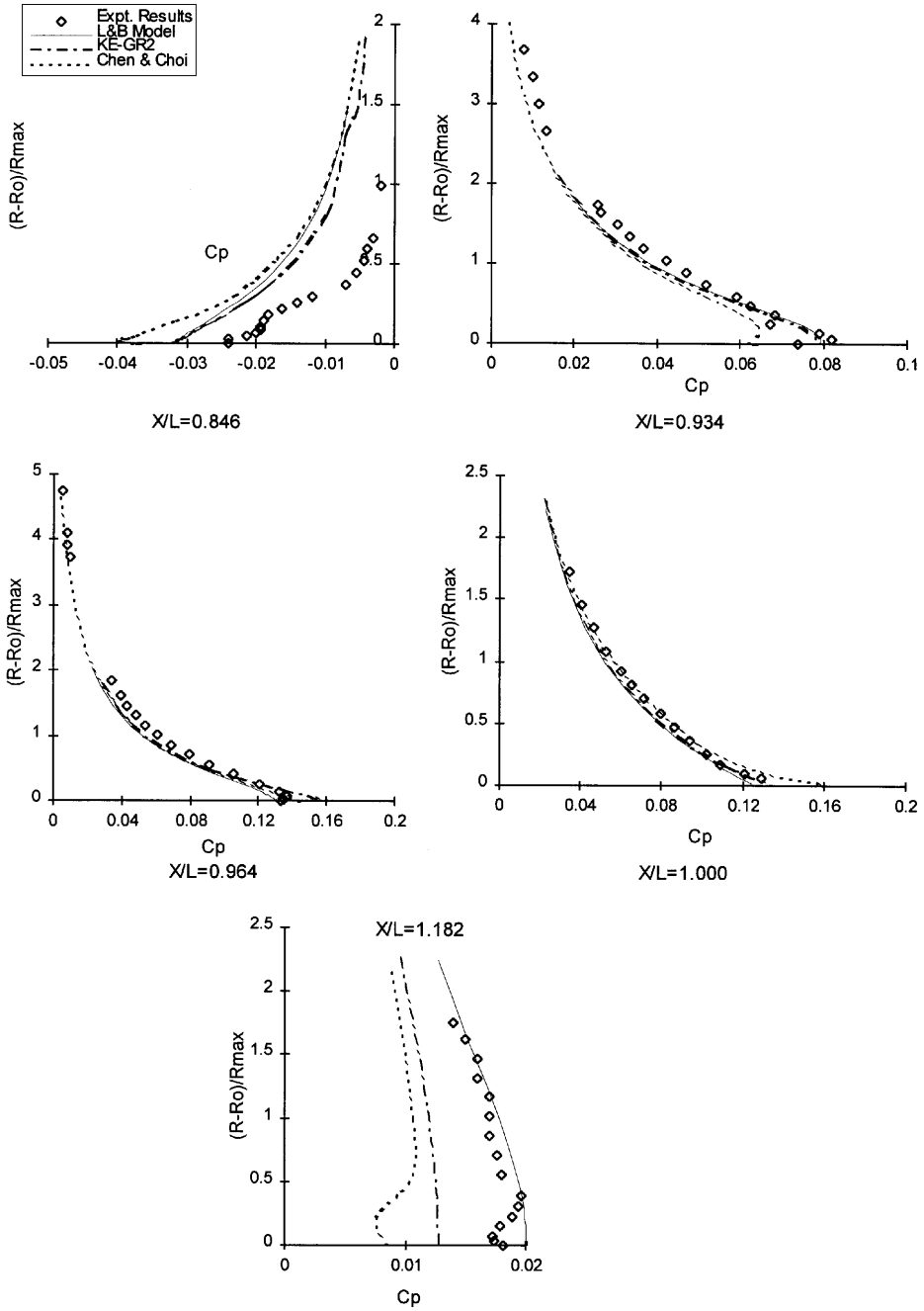

Figure 7. Pressure profiles for AFTERBODY1

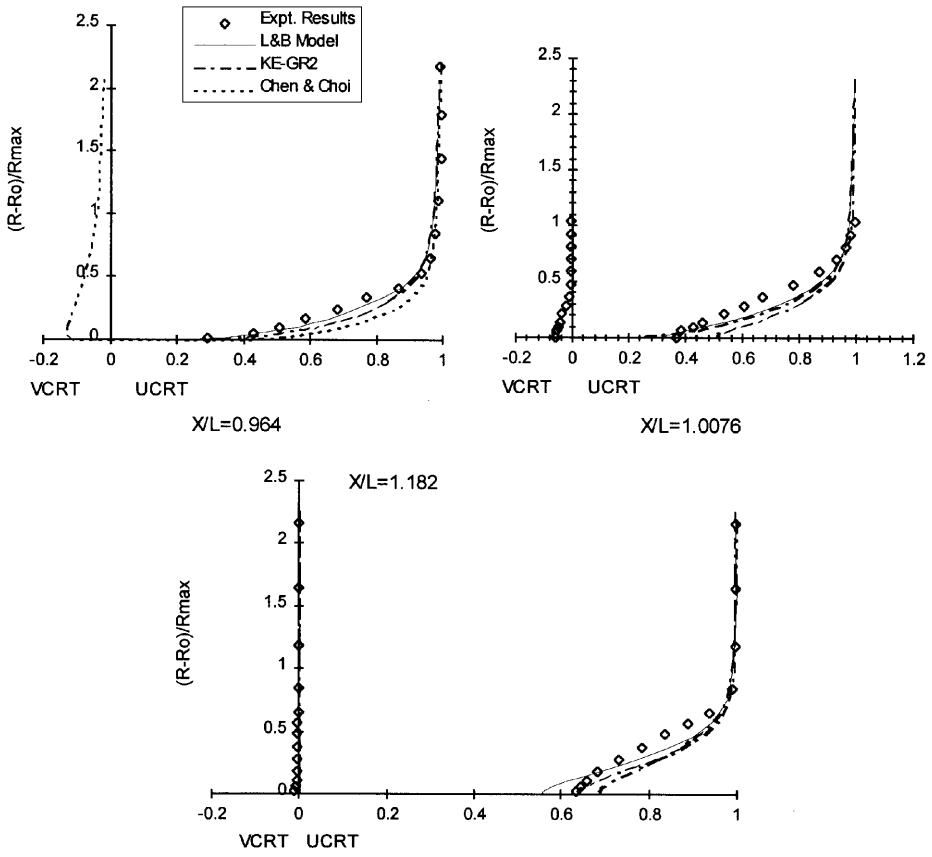

Figure 8. Velocity profiles for AFTERBODY1

Table IV. Volumetric drag coefficients for AFTERBODY1

Turbulence model	C_{pv}	C_{fv}	C_{dv}
Standard k–ε model	0·0027	0·0297	0·0324
L&B model	0·0023	0·0270	0·0293
L&B model with Yap corrections	0·0022	0·0225	0·0247
Experimental results	—	—	0·0276
ESDU	0·0017	0·0260	0·0277

Table V. Volumetric drag coefficients for AFTERBODY2

Turbulence model	C_{pv}	C_{fv}	C_{dv}
Standard k–ε model	0·0041	0·0304	0·3454
L&B model	0·0024	0·0261	0·0285
L&B model with Yap corrections	0·0024	0·0257	0·0281
Experimental results	—	—	0·0280
ESDU	0·0018	0·0258	0·0277

Table VI. Volumetric drag coefficients for MS

Turbulence model	C_{pv}	C_{fv}	C_{dv}
Standard k–ε model	0·0026	0·0334	0·0360
L&B model	0·0015	0·0178	0·0193
L&B model with Yap corrections	0·0015	0·0178	0·0193
ESDU	0·0067	0·0257	0·0324

Table VII. Volumetric drag coefficients for F- 57

Turbulence model	C_{pv}	C_{fv}	C_{dv}
Standard k–ε model	0·0085	0·0335	0·0420
L&B model	0·0078	0·0245	0·0323
L&B model with Yap corrections	0·0078	0·0245	0·0323
ESDU	0·0067	0·0257	0·0324

The comparative analysis of the results in the above paragraphs shows that the present method using the low-*Re* L&B model of turbulence and judicious application of the Yap corrections can be successfully used to predict the flow past a wide range of axisymmetric AUV hull forms. The results obtained are of reasonable accuracy for use in design, particularly for a comparative analysis of a large number of hull forms. Computationally the present method has been shown to be efficient. Furthermore, only a minor adjustment of the solution control parameters is required to achieve numerical stability and convergence even for the wide range of geometries tested here. Hence it is felt that the present method can offer a cost-effective alternative, particularly at the conceptual stages of selecting a hull form, a process which normally requires the assessment of a large number of alternatives.

CONCLUSIONS

Using the general-purpose CFD software PHOENICS, a new computationally efficient and numerically robust flow simulation technique has been developed for axisymmetric AUVs. Application to a wide range of geometries has demonstrated that the method is sufficiently accurate for design purposes and that it could be used to reduce costs significantly during the early stages of design. It has also been shown that for simulation of the flow past axisymmetric AUVs the low-*Re* L&B model of turbulence with judicious application of the Yap corrections improves considerably the flow predictions in comparison with the standard k–ε model using wall functions.

ACKNOWLEDGEMENTS

The first author wishes to express his sincere gratitude to the Government of India for supporting this study through the Ministry of Human Resource Development.

APPENDIX: NOMENCLATURE

C_{dv} volumetric total drag coefficient ($D/\frac{1}{2}\rho V^{2/3}U^2$)
C_{fv} volumetric friction drag coefficient ($F/\frac{1}{2}\rho V^{2/3}U^2$)
C_p surface pressure coefficient ($P_d/\frac{1}{2}\rho U^2$)

C_{pv}	volumetric pressure drag coefficient ($P/\frac{1}{2}\rho V^{2/3}U^2$)
D	total drag force on body
F	friction drag of body
k	turbulent kinetic energy
L	length of body
P	pressure drag of body
P_d	local dynamic pressure
Re	Reynolds number based on length
u	velocity component in axial direction
u_τ	resultant friction velocity
U	velocity of body
U_i	velocity vector
UCRT	axial component of velocity
v	velocity component in radial direction
V	volume of body
VCRT	radial component of velocity
X	axial distance from nose
y	normal distance from body surface
y^+	dimensionless distance normal to body surface, defined as $y^+ = yu_\tau/v$.

REFERENCES

1. V. C. Patel and H. C. Chen, 'Flow over tail and in wake of axisymmetric bodies: review of the state of the art', *J. Ship Res.*, **30**, 201 (1986).
2. S. B. Park, M. K. Chung and D. H. Choi, 'Reynolds-stress model analysis of turbulent flow over a curved axisymmetric body', *AIAA J.*, **29**, 591 (1991).
3. S. K. Choi and C. J. Chen, 'Navier–Stokes solution of complex turbulent flow past finite axisymmetric bodies', *AIAA J.*, **29**, 998 (1991).
4. C. K. G. Lam and K. A. Bremhorst, 'Modified form of k–ε model for predicting wall turbulence', *J. Fluids Eng.*, **103**, 456 (1981).
5. S. H. Crandall, *Engineering Analysis*, Kruger, Malabar, FL, 1983.
6. B. E. Launder and D. B. Spalding, 'The numerical computation of turbulent flows', *Comput. Methods Appl. Mech. Eng.*, **3**, 269 (1974).
7. S. V. Patankar, *Numerical Heat Transfer and Fluid Flow*, McGraw-Hill, New York, 1980.
8. D. B. Spalding, 'Mathematical modelling of fluid mechanics, heat transfer and chemical reaction processes', *CFDU Rep. HTS/80/1*, Imperial College, London, 1980.
9. T. Sarkar, 'Simulation of the flow past axisymmetric underwater vehicles', *Ph.D. Thesis*, University of Strathclyde, Glasgow, 1995.
10. T. T. Huang, N. Santelli and G. Belt, 'Boundary layer flow on axisymmetric bodies', *Proc. 12th ONR Symp. on Naval Hydrodynamics*, Washington, DC, 1978, pp. 127–157.
11. V. C. Patel and Y. T. Lee, 'Thick axisymmetric boundary layer and near wake of a low drag body of revolution', *IIHR Rep. 210*, Iowa Institute of Hydraulic Research, 1977.
12. V. C. Patel, A. Nakayama and R. Damian, 'Measurements in the thick axisymmetric boundary layer near the tail of a body of revolution', *J. Fluid Mech.*, **63**, 345 (1974).
13. C. R. Maliska and G. D. Raithby, 'A method for computing three-dimensional flows using non-orthogonal boundary-fitted co-ordinates', *Int. j. numer. methods fluids*, **4**, 519 (1984).
14. C. Yap, 'Turbulent heat and momentum transfer in recirculating and impinging flows', *Ph.D. Thesis*, University of Manchester, 1987.
15. ESDU, 'Profile drag of axisymmetric bodies at zero incidence for subcritical mach numbers', *ESDU 78019*, 1978.

